Preheating ablation effects on the Rayleigh–Taylor instability in the weakly nonlinear regime

Cite as: Phys. Plasmas **17**, 122706 (2010); https://doi.org/10.1063/1.3517606
Submitted: 22 June 2010 . Accepted: 28 October 2010 . Published Online: 10 December 2010

L. F. Wang, W. H. Ye, Z. M. Sheng, Wai-Sun Don, Y. J. Li, and X. T. He

Preheating ablation effects on the Rayleigh–Taylor instability in the weakly nonlinear regime

L. F. Wang,[1,2,3] W. H. Ye,[2,4,a)] Z. M. Sheng,[5] Wai-Sun Don,[3] Y. J. Li,[1] and X. T. He[2,4]
[1]*SMCE, China University of Mining and Technology, Beijing 100083, People's Republic of China*
[2]*CAPT, Peking University, Beijing 100871, People's Republic of China and LCP, Institute of Applied Physics and Computational Mathematics, Beijing 100088, People's Republic of China*
[3]*Department of Mathematics, Hong Kong Baptist University, Kowloon Tong, Hong Kong*
[4]*Department of Physics, Zhejiang University, Hangzhou 310027, People's Republic of China*
[5]*Beijing National Laboratory for Condensed Matter Physics, Institute of Physics, CAS, Beijing 100190, People's Republic of China and Department of Physics, Shanghai Jiao Tong University, Shanghai 200240, People's Republic of China*

(Received 22 June 2010; accepted 28 October 2010; published online 10 December 2010)

The two-dimensional Rayleigh–Taylor instability (RTI) with and without thermal conduction is investigated by numerical simulation in the weakly nonlinear regime. A preheat model $\kappa(T)=\kappa_{SH}[1+f(T)]$ is introduced for the thermal conduction [W. H. Ye, W. Y. Zhang, and X. T. He, Phys. Rev. E **65**, 057401 (2002)], where κ_{SH} is the Spitzer–Härm electron thermal conductivity coefficient and $f(T)$ models the preheating tongue effect in the cold plasma ahead of the ablation front. The preheating ablation effects on the RTI are studied by comparing the RTI with and without thermal conduction with identical density profile relevant to inertial confinement fusion experiments. It is found that the ablation effects strongly influence the mode coupling process, especially with short perturbation wavelength. Overall, the ablation effects stabilize the RTI. First, the linear growth rate is reduced, especially for short perturbation wavelengths and a cutoff wavelength is observed in simulations. Second, the second harmonic generation is reduced for short perturbation wavelengths. Third, the third-order negative feedback to the fundamental mode is strengthened, which plays a stabilization role. Finally, on the contrary, the ablation effects increase the generation of the third harmonic when the perturbation wavelengths are long. Our simulation results indicate that, in the weakly nonlinear regime, the ablation effects are weakened as the perturbation wavelength is increased. Numerical results obtained are in general agreement with the recent weakly nonlinear theories as proposed in [J. Sanz, J. Ramírez, R. Ramis *et al.*, Phys. Rev. Lett. **89**, 195002 (2002); J. Garnier, P.-A. Raviart, C. Cherfils-Clérouin *et al.*, Phys. Rev. Lett. **90**, 185003 (2003)].
 [doi:10.1063/1.3517606]

I. INTRODUCTION

A major goal of inertial confinement fusion (ICF) program is to initiate self-sustained fusion reaction at the core of a deuterium-tritium filled spherical capsule. It has long been recognized that the Rayleigh–Taylor instability (RTI), where an interface separating a heavier density material above a lighter density material under an acceleration (for example, gravity), poses severe challenges in achieving ICF autoignition and eventual self-sustained fusion reaction.[1,2] At the initial acceleration stage, when the imploding shell is accelerated inward by the low-density blow-off plasma, the outer shell surface becomes unstable to the RTI. Moreover, at the later stage, when the compressed fuel begins to decelerate the imploding pusher, the inner shell surface is prone to the instability.[1,2] This inherent physical instability can limit the implosion velocity and the drive energy and, in some cases, even break up the implosion shell during the acceleration stage. Furthermore, the instability would hinder the formation of hot spot resulting in the autoignition failure or destruction of ignition hot spot during the deceleration stage. Thus, the ICF target capsule should be designed in such a way that would minimize the growth of the instability at an acceptable level. In this report, the term instability refers to the RTI unless stated otherwise.

It is well-known in the literature that the density gradient effect reduces the RTI growth rate, which is approximated as $\gamma_L=\sqrt{Akg/(1+AkL_m)}$, where $A=(\rho_1-\rho_2)/(\rho_1+\rho_2)$ is the Atwood number, $\rho_1>\rho_2$ are the densities of the fluids, $L_m=\min[|\rho/(\partial\rho/\partial x)|]$ is the minimum density gradient scale length, g is the acceleration, and $k=2\pi/\lambda$ is the perturbation wave number for a given perturbation wavelength λ at the interface of two fluids.[1,3–6]

When the thermal conduction is included in the modeling of the physical system, the instability is referred to as the ablative Rayleigh–Taylor instability (ARTI) as opposed to the classical Rayleigh–Taylor instability (CRTI) in the absence of the thermal conduction. Several analysis in the past studied the instability of the ablation front.[7–17] It has been shown that the ablation effect tends to stabilize the ARTI and a cutoff wavelength λ_c appears when the perturbation wavelength λ is sufficiently short. The linear growth rate derived by Bodner and Takabe,[10,11] $\gamma_T=\alpha\sqrt{kg/(1+kL_m)}-\beta kv_a$, generally agrees with the two-dimensional numerical

a)Author to whom correspondence should be addressed. Electronic mail: ye_wenhua@iapcm.ac.cn.

simulations[12] and experiments,[13] where L_m is the minimum density gradient scale length at the ablation surface, and v_a is the ablation velocity. The two parameters α and β depend on the flow parameters with $\alpha=0.9-0.95$ and $\beta=1-3$ typically.[13–15]

In direct-driven ICF experiments,[14,15] it has been shown that the growth rate of the areal density perturbation is significantly reduced when compared with the LASNEX numerical simulation results if the thermal conduction term using the Spitzer–Härm (SH) electron thermal conductivity[18] is included. Glendinning *et al.*[14] recognized that the difference between the experiment and the LASNEX simulation is due to a change in the longitudinal density profile resulting from preheat by energetic electrons originating in the plasma corona which penetrates beyond the ablation front. In addition, the experiments of Shigemori[15] and Sakaiya *et al.*[16] suggested that the nonlocal electron heat transport plays an important role in the suppression of ARTI at the ablation front. Subsequently, Ye *et al.*[17] found that the ARTI growth rate, $\gamma_{mL}=\sqrt{Akg/(1+AkL_m)}-2kv_a$, agrees well with the experiments and simulations and is a suitable model for the preheating case in direct-drive ICF experiments. The resulting density profile in direct-drive ICF experiments[19] and simulations[14,16] indicated that the estimation of the ablative density gradient length scale L_m is markedly improved when the preheating ablation effect is also taken into account. It should be noted that the first term in γ_T and γ_{mL} can be understood as the density gradient stabilization from the ablation effect, which plays an important role in one of the physical reasons for the stabilization mechanisms of the ICF system.

The physical origin of the dominant stabilizing effect of RTI has been attributed to the so-called ablation stabilization (the removal of modulated material by ablation),[10] overpressure stabilization,[20–23] anisotropic thermal diffusion stabilization,[24] etc. In previous studies where all physics were included have made it difficult to identify and isolate the relevant and dominant physical mechanism responsible for the stabilization effect. In this study, the influence of the ablation in the stabilization of the ARTI is isolated. For comparison, the results will be compared with those obtained from the simulations of the CRTI using the same density profile in the weakly nonlinear regime when the density maintains as a single value function along the direction of the acceleration.

The paper is organized as the following. In Sec. II, the mathematical framework and numerical setup are presented. The governing equations with an addition of the second order thermal conduction term to the energy equation, along with an auxiliary equation for the thermal conductivity are presented. The numerical methods, namely, the classical fifth order weighted essentially nonoscillatory (WENO) finite difference scheme for the inviscid fluxes and the fourth order implicit central finite difference scheme for the temperature equation in the case of ARTI, employed and initial setup of the problem in this study are briefly described. Section III presents some recent analytical study of evolution of the growth of the amplitude of the harmonics of the interface with increasing initial perturbation wavelengths in the weakly nonlinear regime. The harmonic generation coefficients of the first three harmonics are defined and their roles on the weakly nonlinear behaviors of the RTI will be examined in the next section. In Sec. IV, numerical results from simulations of a single-mode sinusoidal perturbed interface with different perturbation wavelengths are presented and discussed for both the ARTI and the CRTI in the weakly nonlinear regime. The thermal conduction effects on the RTI in the weakly nonlinear regime are presented in term of the evolutions of amplitude of the harmonics of the interface in the ARTI and the CRTI simulations. Concluding remarks are given in Sec. V.

II. NUMERICAL METHODS AND INITIAL CONDITION SETUP

A. Governing equations

In this study, the physical system is modeled via the two-dimensional inviscid one-temperature single-fluid with a bulk acceleration force in a constantly accelerating frame of reference.[25]

$$\frac{\partial \rho}{\partial t}+\nabla\cdot(\rho \boldsymbol{u})=0,$$

$$\frac{\partial(\rho \boldsymbol{u})}{\partial t}+\nabla\cdot(\rho \boldsymbol{u}\boldsymbol{u})+\nabla P=\rho \boldsymbol{g}, \tag{1}$$

$$\frac{\partial E}{\partial t}+\nabla\cdot[(E+P)\boldsymbol{u}]=\nabla\cdot(\kappa\nabla T)+\rho \boldsymbol{u}\cdot\boldsymbol{g},$$

where $\rho(\mathrm{g/cm^3})$, $\boldsymbol{u}(\mathrm{cm}/\mu\mathrm{s})$, $T(\mathrm{MK})$, and $\boldsymbol{g}(\mathrm{cm}/\mu\mathrm{s}^2)$ are, respectively, the density, velocity, temperature, and acceleration. $E=c_v\rho T+(1/2)\rho \boldsymbol{u}\cdot\boldsymbol{u}$ is the total energy, $P=\Gamma\rho T(\mathrm{Mbar})$ is the pressure, $c_v=\Gamma/(\bar{\gamma}-1)$ is the specific heat at constant volume. For the CH material used in this study, $\bar{\gamma}=5/3$ and $c_v=86.2713(\mathrm{cm}/\mu\mathrm{s})^2\mathrm{MK}^{-1}$ are used.

The term of $\nabla\cdot(\kappa\nabla T)$ is used to model the electron thermal conduction. The thermal conductivity coefficient $\kappa(T)=\kappa_{\mathrm{SH}}[1+f(T)]$ is introduced,[17] where κ_{SH} is the Spitzer–Härm electron thermal conductivity[18] and $f(T)$ models the preheating tongue effect in the cold plasma ahead of the ablation front. For temperatures $T>0.1$ MK, it has been shown that the ARTI growth rate, the density, and temperature profiles at the ablation front obtained from the $f(T)=\alpha T^{-1}+\beta T^{-3/2}$, agree well with the numerical simulations and the experiments.[17] In this paper, we choose a medium preheat case with parameters $\alpha=8.6$ and $\beta=1.6$. In simulating the CRTI, we set $\kappa_{\mathrm{SH}}=0$.

B. Numerical methods

The physical domain is rectangular. The domain in the x direction is $[x_l,x_r]=[-46.3\ \mu\mathrm{m}, 121.7\ \mu\mathrm{m}]$ with length $L_x=168\ \mu\mathrm{m}$. The domain in the y direction is assumed to be periodical with length $L_y=\lambda$, where λ is the perturbation wavelength of the single-mode sinusoidal interface perturbation. The free-stream boundary conditions are imposed at both ends of the domain in x since the flow is essentially unchanged near the boundaries of the computational domain

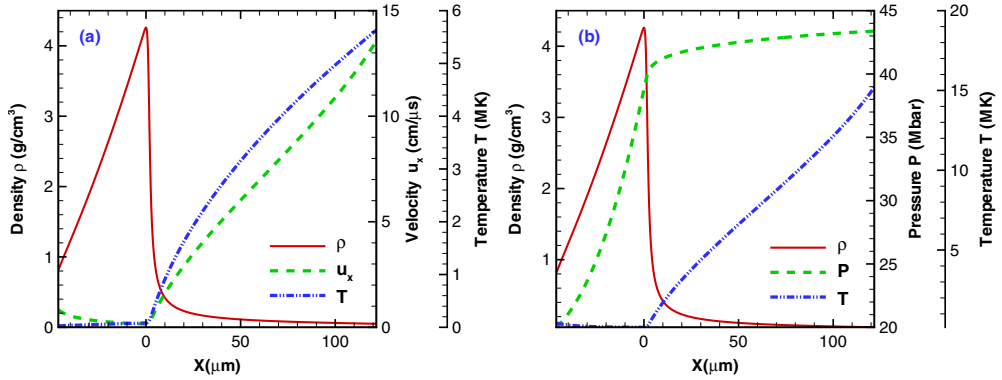

FIG. 1. (Color online) Distributions of the one-dimensional basic flows for the ARTI (a) and the CRTI (b). The two cases have the identical density profiles. The minimum scale length of density gradient at the ablation surface is $L_m=1.83\ \mu$m.

for a sufficiently large domain. Since the domain in y is periodical, periodical boundary conditions are imposed on the upper and lower boundaries.

To simplify the notation for discussion below, the system of partial differential equations can be expressed in the form of

$$\mathbf{Q}_t + L\mathbf{Q} = L_v\mathbf{Q} + \mathbf{S}, \tag{2}$$

where L and L_v are the spatial differential operators for the first (inviscid, nonlinear, hyperbolic) and second order (linear, parabolic) terms, respectively, and $\mathbf{S}$ is the bulk force source term.

We approximate the inviscid flux $L\mathbf{Q}$ in Eq. (2), which is the classical Euler equations, via the well-known classical fifth order characteristic-based weighted essentially nonoscillatory conservative finite difference scheme (WENO) explicitly. Following Refs. 26–28, the hyperbolicity of the Euler Eqs. (2) admits a complete set of right and left eigenvectors for the Jacobian of the system. The eigenvalues and eigenvectors are obtained via the Roe linearized Riemann solver.[29] The first order Lax–Friedrichs flux is used as the low order building block for the high order reconstruction step of the WENO scheme. After projecting the positive and negative fluxes on the characteristic fields via the left eigenvectors, the high order WENO reconstruction step is applied to obtain the high order approximation at the cell boundaries using the surrounding cell-centered values, which are then projected back into the physical space via the right eigenvectors and added together to form a high order numerical flux at the cell-interfaces. The conservative difference of the reconstructed high order fluxes can then be computed for inviscid first order term $L\mathbf{Q}$. We refer to Ref. 28 for further details on the WENO algorithm for solving the hyperbolic conservation laws.

In the case that the thermal conductivity coefficient $\kappa(T)\neq 0$ as in the ARTI, the second order parabolic term involving the thermal conduction is solved via a fourth order implicit central finite difference scheme to avoid the small time step restriction due to the severe stability condition imposed if solved by an explicit scheme. In the simulations presented in Sec. IV, the number of uniformly spaced grid points used in the x and y directions are $N_x=1680$ and $N_y=512$, respectively.

C. Initial condition setup

With the ARTI, the one-dimensional steady state flow field is obtained by integrating Eq. (1) in the accelerating reference frame of the ablation front from the peak density to the isothermal sonic points on both sides of the ablation front[30] (see the left figure of Fig. 1) using the averaged ablation parameters, the peak density $\rho_a=4.3\ \mathrm{g/cm^3}$, the ablation velocity $v_a=1.6\ \mu\mathrm{m/ns}$, the temperature at the peak density $T_a=8.4\times10^{-2}$ MK, and the acceleration $g=17\ \mu\mathrm{m/ns^2}$. With the CRTI, the density profile (see the right figure of Fig. 1) is identical to the one for the ARTI but the pressure profile is computed via the hydrostatic equation $P=P_0+\int_{x_l}^{x_r}\rho g dx$ with hydrostatic pressure $P_0=20$ Mbar.

The primitive variables (ρ,u,v,T) of the initial steady flow field is perturbed with a single-mode sinusoidal interface perturbation at $x=x_0$ with wavelength λ and amplitudes η_0 in the y direction, namely,

$$S(x,y) = 1 + \eta_0 e^{-k_0|x-x_0|}\sin(k_0 y), \tag{3}$$

where $x_0=0$ is the location of the interface and $k_0=2\pi/\lambda$ is the wave number. The amplitude of the perturbation η_0 is typically set as a fraction of wavelength $\eta_0=\alpha_0\lambda$ with $1/10000\leq\alpha_0\leq 1/1000$. For example, the initial perturbed density field $\rho(x,y,t=0)$ becomes $\rho(x,y,0)=\rho_0(x,y)S(x,y)$, where $\rho_0(x,y)$ is the unperturbed initial steady density field.

III. ANALYTICAL HARMONIC ANALYSIS

The *linear* growth regime is defined by $k\eta(t)$ being small (typically $k\eta(t)<0.628$), where $\eta(t)$ represents the typical spatial amplitude of the perturbed interface at time t. (The explicit dependent of η in time t will be dropped for simplicity sake.) After sufficient growth of the perturbation due to the instability, $k\eta$ is no longer small (typically $k\eta\sim 1$) and the flow enters the *nonlinear* regime. Before the strong nonlinear growth regimes, one has the *weakly nonlinear* growth regime.

In the weakly nonlinear growth regime, for a single-mode sinusoidal interface perturbation, within the framework of third-order perturbation theory,[1,25,31–34] the perturbation amplitudes of fundamental mode (first harmonic) η_1, second harmonic η_2, and third harmonic η_3 can be expressed as

$$\eta_1 = \eta_L - \tfrac{1}{16}(3A^2+1)k^2\eta_L^3,$$
$$\eta_2 = \tfrac{1}{2}Ak\eta_L^2, \quad (4)$$
$$\eta_3 = \tfrac{1}{2}\left(A^2-\tfrac{1}{4}\right)k^2\eta_L^3,$$

where $\eta_L = \eta_0 e^{\gamma t}$ and γ are the spatial amplitude and growth rate in the linear regime, respectively. For problems with large Atwood number $A \to 1$, Eq. (4) reduce to[1,25,31–34]

$$\eta_1 = \eta_L - \tfrac{1}{4}k^2\eta_L^3,$$
$$\eta_2 = \tfrac{1}{2}k\eta_L^2, \quad (5)$$
$$\eta_3 = \tfrac{3}{8}k^2\eta_L^3.$$

It should be noted that the above potential expansion theories[31,32] are based on the assumptions that the interface between the two fluids is discontinuous and the thermal conduction is ignored. In ICF experiments, the thermal conduction is inevitable and a smooth mixing layer[19] is formed by the nonlocal electron heat transport or preheat effect of the hot electron, etc. It is, therefore, natural and important to investigate the growth of RTI with a smooth density profile. To investigate the effects of the smooth density transition layer and the ablation on the mode coupling process in the RTI, we generalize Eq. (5) by defining the second harmonic generation coefficient $C(2k)$, third harmonic generation coefficient $D(3k)$, and third-order feedback to the fundamental mode coefficient $E(k)$ and rewrite Eq. (4) as

$$\eta_1 = \eta_L - \tfrac{1}{4}E(k)k^2\eta_L^3,$$
$$\eta_2 = \tfrac{1}{2}C(2k)k\eta_L^2, \quad (6)$$
$$\eta_3 = \tfrac{3}{8}D(3k)k^2\eta_L^3.$$

For long perturbation wavelength ($\lambda \to \infty$), it is expected that Eq. (6) reduce to Eq. (5), or equivalently, one has $C(2k) \to A$, $D(3k) \to (4/3)[A^2-(1/4)]$, and $E(k) \to (1/4)(3A^2+1)$.

Another weakly nonlinear theory for the RTI up to the third-order was also developed by Berning *et al.*[35] which a slightly different form of the growths of the amplitudes of the harmonics was shown. The main reason for the difference between them is that the contribution from linear growth of the second harmonic and the third harmonic is also considered in Ref. 35. According to Eqs. (20) and (40) in Ref. 35, the growths of the second ($n=2$) and third harmonic ($n=3$) described above only consider the growth contribution from mode coupling,[1,25,31–34] i.e., $C_{nn}e^{n\gamma t}$, but drop their corresponding linear growths, i.e., $C_n e^{\sqrt{n}\gamma t}$, where C_{nn} and C_n are typical coefficients in the perturbation amplitudes formulas and $C_{nn} \sim C_n$.[35] In fact, for the growths of the second harmonic and the third harmonic, in a system with a single-mode sinusoidal interface perturbation, one can capture the main growth mechanism by considering the mode coupling growths and ignoring the contributions from their corresponding linear growth since there is $C_{nn}e^{n\gamma t} \gg C_n e^{\sqrt{n}\gamma t}$ within our focus of the weakly nonlinear regime which is typically in the range $0.005\lambda < \eta_3 < \eta_2 < \eta_1 < 0.5\lambda$, where λ is the perturbation wavelength. That is to say, in the present focused weakly nonlinear regime, the growth contribution of the amplitude from the linear growth of the second and third harmonics can be ignored in comparison with the mode coupling growth. Thus it is appropriate to use Eq. (6) in the investigation of RTI in the weakly nonlinear regime in the present research.

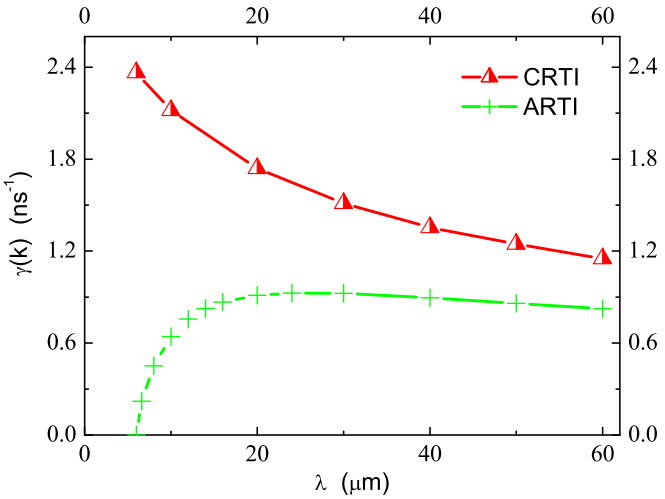

FIG. 2. (Color online) Linear growth rate curves $\gamma(k)$ for the ARTI and the CRTI.

Since the transition between the fluids is no longer sharp, we shall generate a reasonably defined interface in the fluid so that the growth rate of the amplitude of the perturbed interface can be tracked and analyzed by the Fourier analysis in the y direction. For this purpose, we shall define the interface as the location where the density gradient is the largest. In the weakly nonlinear regime where the density $\rho(x,y,t)$ remains as a single value function along the x direction, a function $f(y,t)$ where the density $\rho=2.4$ g/cm^3 can be uniquely defined and its gradient is the largest. Applying the Fourier analysis on the function $f(y,t)$, the absolute values of the Fourier coefficients $\{|a_n(t)|, n=1,\ldots,N_y/2\}$ yield the amplitudes of the nth harmonic of the interface in time t. The linear growth rate γ can then be obtained by fitting the amplitude of the fundamental mode within the linear growth regime. Similarly, the coefficients $\{E(k), C(2k), D(3k)\}$ can be obtained by fitting η_1, η_2, η_3, respectively, within the weakly nonlinear growth regime.

IV. NUMERICAL RESULTS AND DISCUSSIONS

The linear grow rate curves $\gamma(k)$ for the ARTI and the CRTI are plotted in Fig. 2. The result shows that the linear growth rate increases with the decreasing perturbation wavelength λ in the CRTI. However, in the ARTI, the linear growth rate is greatly reduced, especially for the short perturbation wavelength λ. The data also indicates that the cutoff wavelength is $\lambda_c \approx 6$ μm in the ARTI simulation using our medium preheat model.

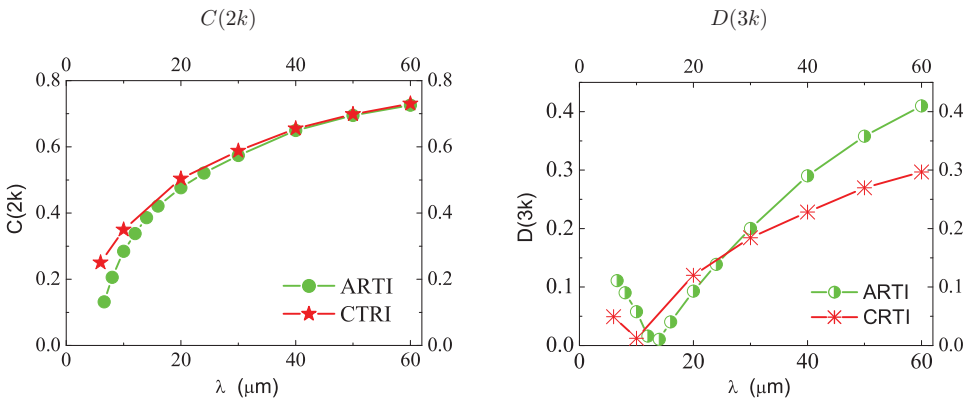

FIG. 3. (Color online) The second $C(2k)$ and third $D(3k)$ harmonic generation coefficients for the ARTI and the CRTI.

A. Ablation effects

To study the weakly nonlinear behaviors of the RTI, we examine the behavior of the second and third harmonic generation coefficients $C(2k)$ and $D(3k)$, respectively, as a function of wave numbers k for both the ARTI and the CRTI in Fig. 3. In the left figure, one can see that the ablation effect has an apparent influence on the coefficient $C(2k)$ of the second harmonic when $\lambda < 20$ μm. The ablation effect is gradually weakened with an increasing perturbation wavelength λ. However, when $\lambda > 40$ μm, the coefficient $C(2k)$ approaches almost the same value for both the ARTI and the CRTI. In the other words, the ablation essentially has no effect on $C(2k)$ for large λ. Moreover, as λ increases, $C(2k) \to A$, which is the classical predicted value for both the ARTI and the CRTI. In the right figure, one can see that the coefficient $D(3k)$ of the third harmonic first decreases and then increases with λ for both the ARTI and the CRTI.

This particular behavior of the coefficient $D(3k)$ has not been predicted by the classical third-order estimation.[31,32,35] To explain this behavior, we analyze the temporal evolution of the amplitudes of the first six harmonics at different perturbation wavelengths λ for both the ARTI and the CRTI. In the ARTI, similar to the CRTI,[25] it appears that:

- With wavelength $\lambda = 10$ μm, the fourth harmonics ($n=4$) is generated earlier than the third harmonic ($n=3$);
- With wavelength $\lambda = 14$ μm, the third and fourth harmonics are generated nearly at the same time, as illustrated in the left figure of Fig. 4; and
- With an increasing λ, the third harmonic in turn is generated earlier than the other higher harmonics ($n \geq 4$).

It is well known that the early generation of the higher harmonics ($n \geq 4$), especially the fourth harmonic, can greatly suppress the generation and the growth of the third harmonic. As noted above, for both the ARTI and the CRTI, the suppression of the third harmonic by the higher harmonics first decreases with wavelength and then increases with it. Accordingly, the $D(3k)$ curve first decreases with perturbation wavelength and then increases with it, as shown in the right figure of Fig. 3. Comparing the ARTI and the CRTI, for the large perturbation wavelength (30 μm$ < \lambda < 60$ μm) and small perturbation wavelengths ($\lambda < 10$ μm), we also find that the suppression of the third harmonic by the higher harmonics is stronger in the CRTI than that in the ARTI. Therefore, $D(3k)$ in the ARTI is greater than that in the CRTI when $\lambda < 10$ μm and 30 μm$ < \lambda < 60$ μm.

Figure 5 shows the coefficient $E(k)$ of the third-order feedback to the fundamental mode for the ARTI and the CRTI. For a short perturbation wavelength λ, $E(k)$ has very different behaviors in the ARTI and the CRTI. In the ARTI, $E(k)$ first decreases and then increases with increasing wave-

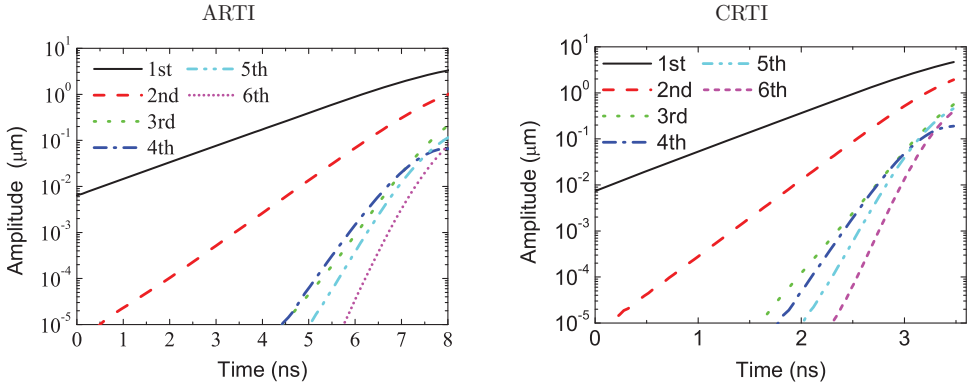

FIG. 4. (Color online) Temporal evolution of the amplitudes of the first six harmonics with a perturbation wavelength $\lambda = 14$ μm for the ARTI and the CRTI using their respective initial conditions, as shown in Fig. 1.

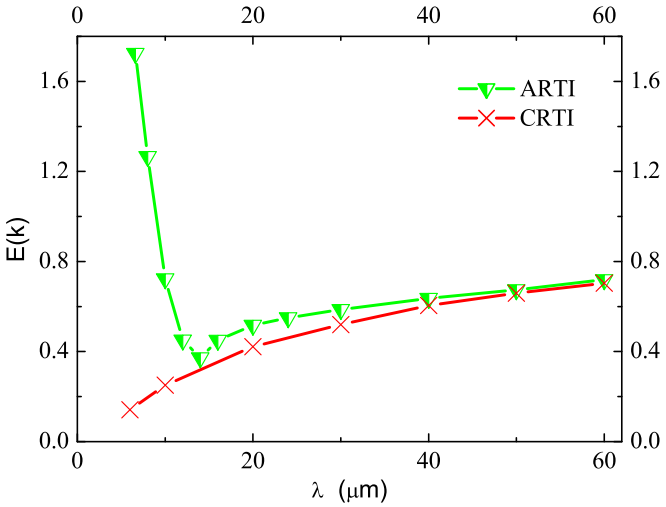

FIG. 5. (Color online) Coefficients of third-order feedback to the fundamental mode $E(k)$ for the ARTI and the CRTI.

length λ and a corresponding minimum wavelength $\lambda_{min}=14$ μm. In the CRTI, however, $E(k)$ increases continuously with decreasing wavelength λ. Comparing the ARTI and the CRTI, we can conclude that the ablation plays a stabilization role since $E(k)$ in the ARTI is greater than that in the CRTI which resulted in the reduction of the amplitude of the fundamental harmonic η_1. In addition, it is noteworthy that for both the ARTI and the CRTI there is $E(k)<1.0$, except for the ARTI when $\lambda \to \lambda_c$. Consequently, the nonlinear saturation amplitude[25] in both the ARTI and the CRTI should be increased and therefore exceeds the classical prediction 0.1λ,[31,32,35] which is harmful for the ICF ignition.

B. Transition layer thickness effects

In order to further identify which effect or effects, such as the nonlinearity, the transition layer thickness or the thermal conduction determines the counter-intuitive behavior, namely, the fourth harmonic growing faster than the third harmonic mentioned above, we present simulations of the CRTI with interface perturbation wavelength $\lambda=14$ μm. Here, the one-dimensional steady flow of the density profile is in the form

$$\rho(x)=\frac{1}{2}(\rho_l+\rho_r)-\left[\frac{1}{2}(\rho_l-\rho_r)\right]\tanh\left(\frac{x}{L_D}\right),$$

where L_D is the typical half-thickness of the density transition layer, where $\rho_l=4.25$ g/cm^3, $\rho_r=0.5$ g/cm^3, with Atwood number $A=0.7895$.[25] The CRTI simulations here are performed with four transition layer half-thicknesses $L_D=0.4$, 0.6, 0.8, and 1.0 μm with the corresponding minimum density gradient scale lengths $L_m=0.31$, 0.47, 0.63, and 0.79 μm. Please note that here the one-dimensional pressure profile is also computed via hydrostatic equation with again $P_0=20$ Mar and $g=17$ μm/ns^2. The temporal evolutions of the amplitudes of the first six harmonics of the simulations are shown in Fig. 6.

For the $\lambda=14$ μm perturbation wavelength, the counter-intuitive behavior of the fourth harmonic growing faster than the third harmonic mentioned above is observed in the ARTI

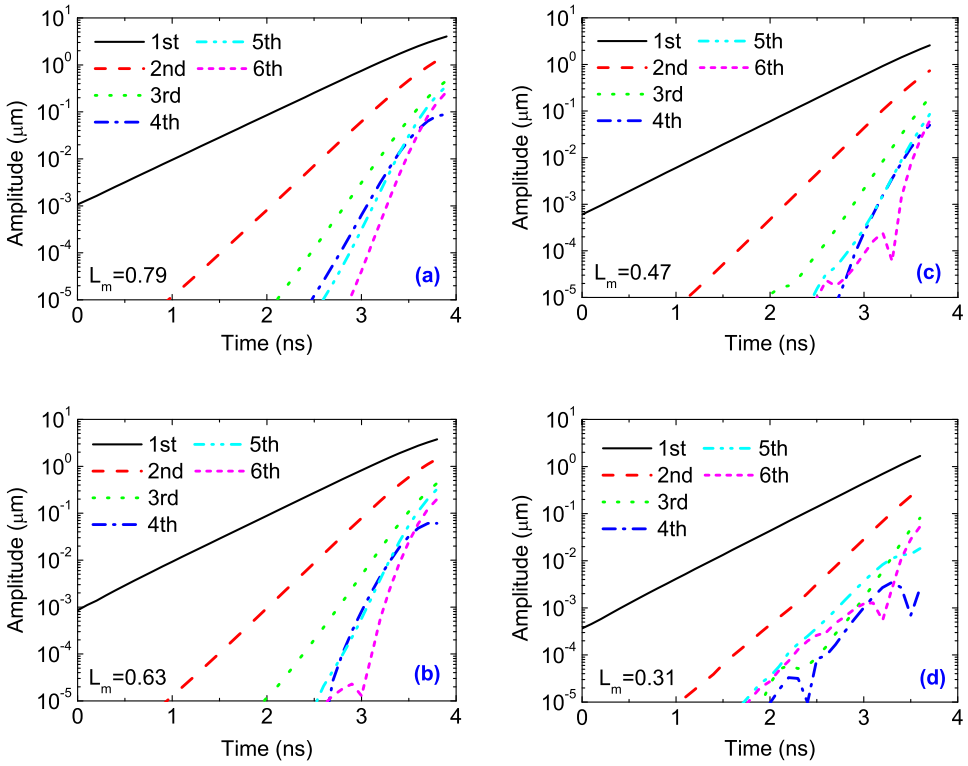

FIG. 6. (Color online) The temporal evolution of the amplitudes of the first six harmonics in the CRTI with a perturbation wavelength $\lambda=14$ μm and the minimum density gradient scale lengths (a) $L_m=0.79$ μm, (b) $L_m=0.63$ μm, (c) $L_m=0.47$ μm, and (d) $L_m=0.31$ μm.

but not in the CRTI where the higher harmonics are generated one by one (see the left and right figure of Fig. 4, respectively). Therefore, one may conclude that the ablation effect strongly influences the mode coupling process and counterintuitive behaviors in the mode coupling process can occur when the effect of the thermal conduction is included. We would also like to point out that, as seen in Fig. 6, counterintuitive behavior with the lower harmonic growing faster than the higher one can also be observed when one decreases the transition layer thickness, L_D. Therefore, the transition layer thickness effect also strongly influences the mode coupling process in the absence of thermal conduction.[25] These results obtained above indicate that both the transition layer thickness L_D and the thermal conduction $\kappa(T)$ play central roles in the mode coupling process in the RTI. Detailed research in these areas will be pursued and reported in our future work.

C. Summary

In summary, for long perturbation wavelength, results obtained in this study are in general agreement with the recent weakly nonlinear theories of ARTI by Sanz and Ganier.[7,8] However, large differences appear as perturbation wavelength λ approaches the cutoff wavelength λ_c. The mode coupling coefficients given by Refs. 7 and 8 can be negative, especially for $E(k)$. This means that the third-order feedback strengthens the growth of the fundamental mode. That is, the fundamental mode cannot be saturated if one only considers the mode coupling process up to the third-order. Obviously, it is nonphysical. In our present work, contrarily, $E(k)$ is always positive. Moreover, the transition layer thickness also plays a key stabilization role in the ARTI growth, especially for the short perturbation wavelength λ in the weakly nonlinear regime. Note that the transition layer thickness effects were not sufficiently addressed in the work by Sanz or Garnier, but are studied in some detail here.

V. CONCLUSION

In this research, we have numerically investigated the two-dimensional RTI with and without thermal conduction (ARTI and CRTI, respectively) in the weakly nonlinear regime. A preheat model for the thermal conductivity is introduced to take into account of the preheating ablation effect of thermal conduction on the ARTI. The system of partial differential equations is solved using the high order weighted essentially non-oscillatory scheme and implicit central finite difference scheme. The preheating ablation effects and the ablation surface thickness effects on the RTI are studied by comparing the ARTI and the CRTI with an identical density profile relevant to inertial confinement fusion experiments.

It is found that the ablation effects dramatically influence the mode coupling process, especially for the short perturbation wavelengths. On the whole, the ablation effects stabilize the ARTI in the weakly nonlinear regime. First, the linear growth rate is reduced, especially for short perturbation wavelengths and a cutoff wavelength is observed in the simulations of the ARTI. Second, the second harmonic generation is reduced for the short perturbation wavelengths and the third-order negative feedback to the fundamental mode is strengthened. All of these factors noted above play a stabilization role on the ARTI in the weakly nonlinear regime. Finally, on the contrary, the ablation effects increase the generation of the third harmonic when the perturbation wavelengths are long. The counterintuitive behaviors with the lower harmonics growing faster than the higher ones are observed in both the ARTI and the CRTI and have been explained by analyzing the temporal evolution of the first six harmonics. Numerical results obtained in the present works are in general agreement with the recent weakly nonlinear theories.[7,8]

In direct-driven experiments in inertial confinement fusion, the jetlike long spikes are formed.[36–39] In the astrophysics, the astrophysical jets can remain well collimated over propagation distances exceeding ten jet diameters or more.[40] Our works show that when the thermal conduction with preheat is considered, the growth of the ARTI is stabilized in the weak nonlinear regime while the nonlinear saturation amplitude is improved, which is expected to improve the understanding of the stabilization factors for the astrophysical jet and of the formation mechanisms for the jetlike long spikes.

ACKNOWLEDGMENTS

The author (L.F.W.) would like to thank Professor S. Atzeni (Università di Roma "La Sapienza" and CNISM) and Professor K. Nishihara (Osaka University) for their helpful discussions and the anonymous referee for suggestions that have improved the paper. This research was supported by the National Basic Research Program of China (Grant No. 2007CB815100) and the National Natural Science Foundation of China (Grant Nos. 10935003, 11075024, 10905006, and 11074300). Both authors (W.S.D. and L.F.W.) would like to thank the support provided by the RGC grant from Hong Kong Research Grants Council. The author (L.F.W.) also would like to acknowledge the hospitality of the Department of Mathematics at Hong Kong Baptist University during his visit while conducting the research reported here.

[1] J. D. Lindl, P. Amendt, R. L. Berger, S. G. Glendinning, S. H. Glenzer, S. W. Haan, R. L. Kauffman, O. L. Landen, and L. J. Suter, Phys. Plasmas **11**, 339 (2004).
[2] S. Atzeni and J. Meyer-ter-Vehn, *The Physics of Inertial Fusion: Beam Plasma Interaction, Hydrodynamics, Hot Dense Mater* (Oxford Univeristy Press, Oxford, 2004).
[3] K. O. Mikaelian, Phys. Rev. Lett. **48**, 1365 (1982).
[4] K. O. Mikaelian, Phys. Rev. A **40**, 4801 (1989).
[5] A. B. Bud'ko and M. A. Liberman, Phys. Fluids B **4**, 3499 (1992).
[6] L. F. Wang, W. H. Ye, and Y. J. Li, Phys. Plasmas **17**, 042103 (2010).
[7] J. Sanz, J. Ramírez, R. Ramis, R. Betti, and R. P. J. Town, Phys. Rev. Lett. **89**, 195002 (2002).
[8] J. Garnier, P.-A. Raviart, C. Cherfils-Clérouin, and L. Masse, Phys. Rev. Lett. **90**, 185003 (2003).
[9] T. Ikegawa and K. Nishihara, Phys. Rev. Lett. **89**, 115001 (2002).
[10] S. Bodner, Phys. Rev. Lett. **33**, 761 (1974).
[11] H. Takabe, K. Mima, L. Montierth, and R. L. Morse, Phys. Fluids **28**, 3676 (1985).
[12] M. Tabak, D. H. Munro, and J. D. Lindl, Phys. Fluids B **2**, 1007 (1990).
[13] H. Azechi, T. Sakaiya, S. Fujioka, Y. Tamari, K. Otani, K. Shigemori, M. Nakai, H. Shiaga, N. Miyanaga, and K. Mima, Phys. Rev. Lett. **98**, 045002 (2007).

[14]S. G. Glendinning, S. N. Dixit, B. A. Hammer, D. H. Kalantat, M. H. Key, J. D. Kilkenny, J. P. Knauer, D. M. Pennington, B. A. Remington, R. J. Wallace, and S. V. Weber, Phys. Rev. Lett. **78**, 3318 (1997).
[15]K. Shigemori, H. Azechi, M. Nakai, M. Honda, K. Meguro, N. Miyanaga, H. Takabe, and K. Mima, Phys. Rev. Lett. **78**, 250 (1997).
[16]T. Sakaiya, H. Azechi, M. Matsuoka, N. Izumi, M. Nakai, K. Shigemori, H. Shiraga, A. Sunahara, H. Takabe, and T. Yamanaka, Phys. Rev. Lett. **88**, 145003 (2002).
[17]W. H. Ye, W. Y. Zhang, and X. T. He, Phys. Rev. E **65**, 057401 (2002).
[18]L. Spitzer and R. Härm, Phys. Rev. **89**, 977 (1953).
[19]S. Fujioka, H. Shiraga, M. Nishikino, K. Shigemori, A. Sunahara, M. Nakai, H. Azechi, K. Nishihara, and T. Yamanaka, Phys. Plasmas **10**, 4784 (2003).
[20]J. Sanz, Phys. Rev. Lett. **73**, 2700 (1994).
[21]A. P. Piriz, J. Sanz, and L. F. Ibañez, Phys. Plasmas **4**, 1117 (1997).
[22]V. N. Goncharov, R. Betti, R. L. McCrory, P. Sorotokin, and C. P. Verdon, Phys. Plasmas **3**, 1402 (1996).
[23]R. Betti, V. N. Goncharov, R. L. McCrory, and C. P. Verdon, Phys. Plasmas **5**, 1446 (1998).
[24]L. Masse, Phys. Rev. Lett. **98**, 245001 (2007).
[25]L. F. Wang, W. H. Ye, and Y. J. Li, Phys. Plasmas **17**, 052305 (2010).
[26]D. Balsara and C. W. Shu, J. Comput. Phys. **160**, 405 (2000).
[27]G. S. Jiang and C. W. Shu, J. Comput. Phys. **126**, 202 (1996).
[28]R. Borges, M. Carmona, B. Costa, and W. S. Don, J. Comput. Phys. **227**, 3191 (2008).
[29]P. L. Roe, J. Comput. Phys. **43**, 357 (1981).
[30]Z. F. Fan, J. S. Luo, and W. H. Ye, Phys. Plasmas **16**, 102104 (2009).
[31]J. W. Jacobs and I. Catton, J. Fluid Mech. **187**, 329 (1988).
[32]S. W. Haan, Phys. Fluids B **3**, 2349 (1991).
[33]B. A. Remington, S. V. Weber, M. M. Marinak, S. W. Haan, J. D. Kilkenny, R. J. Wallace, and G. Dimonte, Phys. Plasmas **2**, 241 (1995).
[34]V. A. Smalyuk, V. N. Goncharov, T. R. Boehly, J. P. Knauer, D. D. Meyerhofer, and T. C. Sangster, Phys. Plasmas **11**, 5038 (2004).
[35]M. Berning and A. M. Rubenchik, Phys. Fluids **10**, 1564 (1998).
[36]D. K. Bradley, D. G. Braun, S. G. Glendinning, M. J. Edwards, J. L. Milovich, C. M. Sorce, G. W. Collins, S. W. Haan, R. H. Page, and R. J. Wallace, Phys. Plasmas **14**, 056313 (2007).
[37]B. A. Remington, S. W. Haan, S. G. Glendinning, J. D. Kilkenny, D. H. Munro, and R. J. Wallace, Phys. Fluids B **4**, 967 (1992).
[38]B. A. Remington, R. P. Drake, H. Takabe, and D. Arnett, Phys. Plasmas **7**, 1641 (2000).
[39]J. O. Kane, H. F. Robey, B. A. Remington, R. P. Drake, J. Knauer, D. D. Ryutov, H. Louis, R. Teyssier, O. Hurricane, D. Arnett, R. Rosner, and A. Calder, Phys. Rev. E **63**, 055401 (2001).
[40]B. Reipurth and J. Bally, Annu. Rev. Astron. Astrophys. **39**, 403 (2001).